Observation of intergranular films in BaB_2O_4-added $BaTiO_3$ ceramics

Joon-Hyung Lee,[a] and Jeong-Joo Kim
Department of Inorganic Materials Engineering, Kyungpook National University, Taegu 702-701, Korea

Haifeng Wang
Department of Materials Science & Engineering, Massachusetts Institute of Technology, Cambridge, Massachusetts 02139

Sang-Hee Cho
Department of Inorganic Materials Engineering, Kyungpook National University, Taegu 702-701, Korea

(Received 11 August 1999; accepted 26 April 2000)

Distribution characteristics of boundary phase in BaB_2O_4 added $BaTiO_3$ ceramics were investigated with a focus on the curvature difference of solid–liquid interfaces at two-grain and triple junctions. High-resolution transmission electron microscopy revealed that the triple junction of solid grains showed the positive curvature of solid–liquid interface and consisted of the mixture of liquid phase and crystallized BaB_2O_4 phase. On the other hand, flat amorphous thin film of 2.5-nm thickness was observed at the two-grain junction. This kind of boundary phase distribution characteristic was explained by the solubility difference between two kinds of junctions of solid grains that had different curvature of solid–liquid interfaces.

I. INTRODUCTION

There has been a significant amount of work towards establishing the relationship between the positive temperature coefficient of resistivity (PTCR) properties of $BaTiO_3$ ceramics and their microstructures, which in turn depends critically on the processing parameter, e.g., sintering profile, atmosphere, additives, etc.[1–3] In general, small amounts of sintering aids such as TiO_2, SiO_2, and Al_2O_3 were usually added to $BaTiO_3$ ceramics for achieving homogeneous microstructure and lowering the sintering temperature through the liquid-phase sintering.[4–6] Recently, Park *et al.*[7] and Ho[8] used BN addition as a sintering aid and Heo *et al.*[9] showed that the BaB_2O_4 compound was the most effective sintering aid of the various boron-containing compounds for low-temperature sintering of $BaTiO_3$ ceramic system.

The liquid-sintered body could be considered a composite of crystalline grains and amorphous liquid phase, and two kinds of distribution characteristics of intergranular liquid phase can be developed in microstructure around the grain boundary during the liquid-phase sintering. One is bulk liquid pocket, which is located at triple or four-grain junctions. The size of liquid pocket is proportional to the grain size and volume fraction of the liquid phase, and its shape is determined by the dihedral angle of the system.[10–12] The other is thin-liquid films at two-grain junction. Its thickness is a few nm order and independent of grain size or liquid amount, and thought to be of an equal value to the composition and temperature.[13–15] Such an intergranular amorphous phase may crystallize during the cooling and adequate annealing process, and the final microstructure and physical properties may also change. This means that the crystallization behaviors of the intergranular amorphous phase are important for a better understanding of microstructure and physical properties of a liquid-phase sintered body.

In this study, BaB_2O_4 compound was used as a sintering aid for lowering the sintering temperature of $BaTiO_3$ ceramics that had PTCR composition, and the phase-distribution characteristics were examined using x-ray diffractometer (XRD) and high-resolution transmission electron microscopy (HRTEM), respectively. The crystallization characteristics of the boundary phase in BaB_2O_4 added $BaTiO_3$ ceramics were discussed with a focus on the curvature difference of solid–liquid interfaces between two-grain and triple junctions.

II. EXPERIMENTAL

Specimens with a PTCR formula of $(Ba_{0.997}Y_{0.003})TiO_3$ were prepared using high purity chemicals of $BaCO_3$(99.94%), TiO_2(99.97%), and Y_2O_3(99.999%).

[a]Address all correspondence to this author.
e-mail: jhlee@icm.re.kr

Raw materials were wet-ball milled for 20 h with ethyl alcohol in a polyethylene jar using zirconia balls and then calcined at 1150 °C for 1 h. The BaB_2O_4 compound was synthesized at 1000 °C using chemical grade $BaCO_3$ and H_3BO_3 powders. The mixture of 8 mol% of BaB_2O_4 and the calcined $(Ba_{0.997}Y_{0.003})TiO_3$ powder was ball milled again for 20 h. The mixed powders were compacted with a hydrostatic pressure of 98 MPa, and sintered at 1150 °C for 1 h in air and then furnace cooled with a rate of about 400 °C/h. For phase identification, XRD (Rigaku, D/MAX 2500, Tokyo, Japan) was used. HRTEM (Topcon EM-002B, Paramus, NJ) studies were accompanied to analyze grain-boundary structure and morphology.

III. RESULTS AND DISCUSSION

Figure 1 shows the microstructure of 8 mol% BaB_2O_4 added to a $BaTiO_3$ specimen sintered at 1150 °C for 1 h. Its microstructure resembles a typical microstructure of PTCR devices without abnormal grain growth. In the BaB_2O_4–$BaTiO_3$ system, BaB_2O_4 forms liquid phase at the eutectic point of 942 ± 3 °C.[16] Therefore, when the samples are sintered at 1150 °C, liquid-phase sintering occurs, which provides a faster diffusion path and accelerates densification. The average grain size was 6.5 ± 1.0 μm, and the apparent density and porosity of the specimen was 5.70 ± 0.12 g/cm^3 and 5.2 ± 2.0%, respectively.

Figure 2 shows the XRD pattern of a 8 mol% BaB_2O_4-added $BaTiO_3$ specimen sintered at 1150 °C for 1 h. Diffraction peaks are completely identical with major peaks of BaB_2O_4 and perovskite $BaTiO_3$ phases, respectively. It was assumed that melts of the BaB_2O_4 compound led to an acceleration of the densification during heating, and was then transformed again to the crystalline phase during the cooling procedure.

Figure 3 shows a HRTEM micrograph of a triple junction (or four-grain junction) of solid grains. The left upper edge of the liquid pocket was preferentially etched out by ion-milling perforation, and lattice fringes of perovskite $BaTiO_3$ solid grains are shown. The interesting part of this micrograph is the lattice fringes of small-crystallized particles are clearly seen within the amorphous liquid pocket. The crystallized particles had aggregated forms with few nanometer-sized crystallites, and the lattice fringes of particles show no special orientation of growth. Because the size of the crystallites was so small and they contained a boron component, the exact composition of crystallites and amorphous liquid was not successfully analyzed. However, considering XRD result and mass balance of specimens, the composition of crystallites and amorphous phase was assumed to be BaB_2O_4 and Ba–Ti–B–O glass phase, respectively. The phase diagram of the BaB_2O_4–$BaTiO_3$ system also confirms the formation of the BaB_2O_4 phase at the entire range of composition below the eutectic temperature of 942 ± 3 °C.[16]

Figure 4 represents a HRTEM micrograph of the two-grain junction region. Along the lattice fringes of grains, thin amorphous liquid film with a thickness about 2.5 nm was observed without any crystalline, even though the liquid at the triple junction was already crystallized as shown in Fig. 3. These amorphous thin films are characterized by being nearly constant in thickness along the boundary with an order of a few nanometers.[13] The thickness is dependent on composition and temperature, etc., and considered to be an equilibrium state as reported in other literatures.[14,15,17] Clarke[13,17] proposed that the thickness of the intergranular film represented the equilibrium separation between grains determined by a balance between attractive (van der Waals force between grains and capillary forces from liquid menisci) and repulsive forces (repulsive electrostatic interaction due to

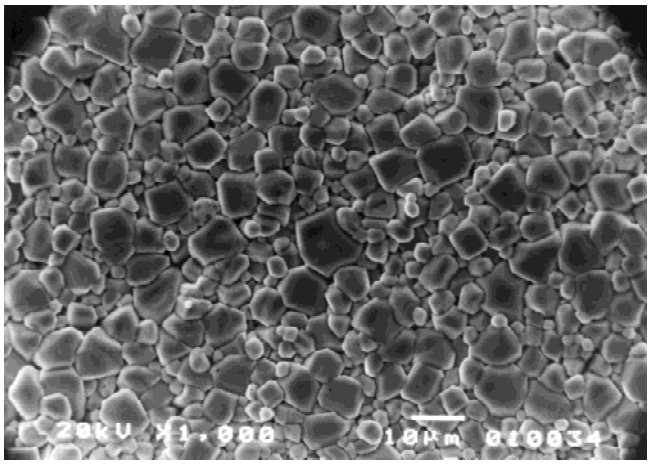

FIG. 1. Microstructure of 8 mol% BaB_2O_4 added $BaTiO_3$-based PTCR sample sintered at 1150 °C for 1 h.

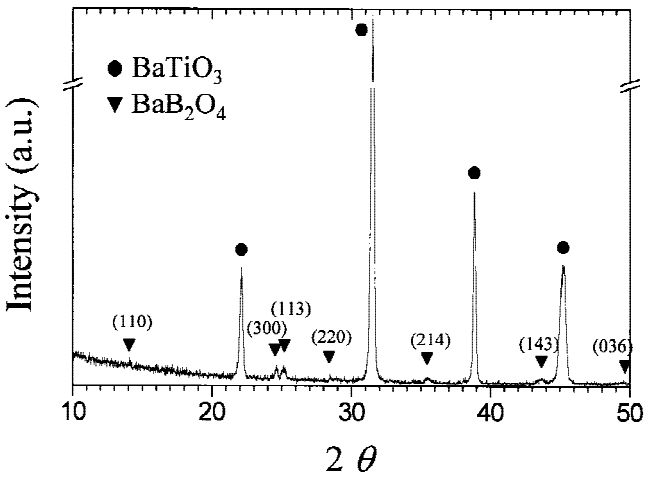

FIG. 2. X-ray diffraction pattern of a 8 mol% BaB_2O_4-added $BaTiO_3$-based PTCR sample sintered at 1150 °C for 1 h.

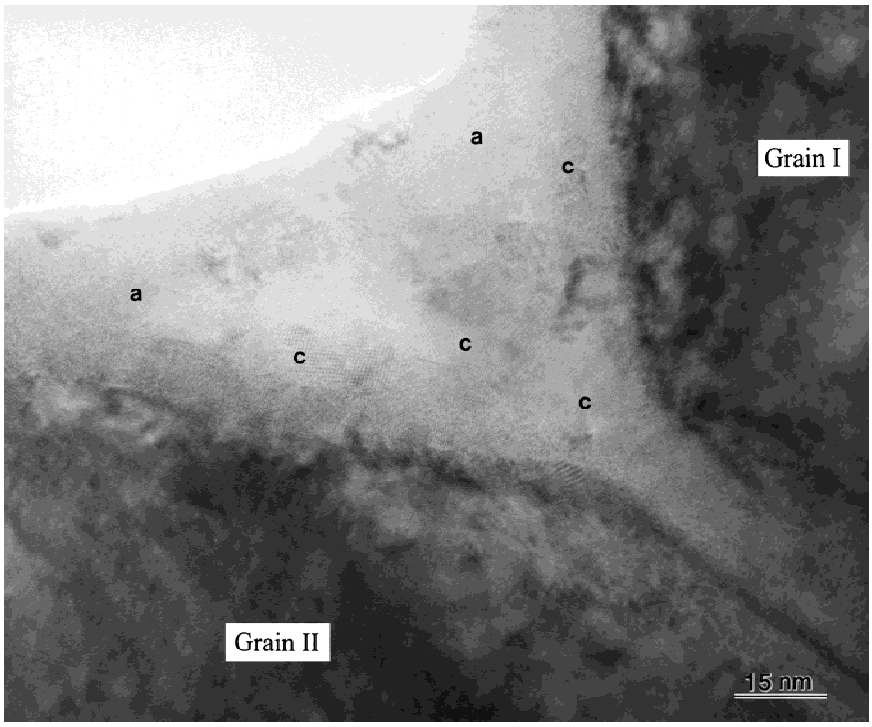

FIG. 3. HRTEM micrograph of triple junction of solid grains. 'a' implies the amorphous and 'c' the crystallized particle.

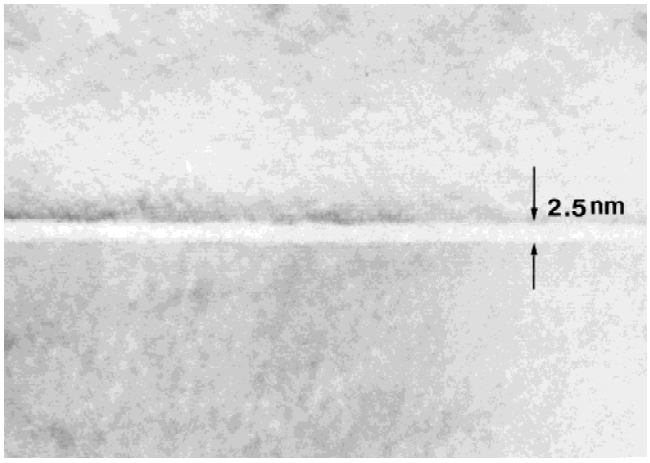

FIG. 4. HRTEM micrograph of two-grain junction region.

charges at the grain/liquid interfaces). But there was no explanation of incomplete crystallization of a glass in two-grain junction.

After Clarke's studies, there were numerous experimental and theoretical studies of boundary films, and several reasons suggested a resistance to crystallization, especially in the thin amorphous film. Raj[18] proposed that a capillary stress due to the curvature of the solid–liquid interface advancing into the film was responsible for a reduction in energy difference between the crystalline and amorphous state of the material. The reduction of this energy difference reduces the driving force for the advancement of the crystallization front into the film. It was also suggested that stresses caused by the volume changes upon crystallization may inhibit complete crystallization.[19–21] However, it seemed unlikely that residual stresses were responsible for the remnant films since there was evidence of sufficient diffusional transport and viscous deformation to relieve such stresses when annealing was performed.[22]

Another explanation for the limitations of boundary film crystallization based on the original Clarke model[13] was proposed.[23] In this explanation, thermodynamic calculations were conducted to model the energy of a liquid constrained between two crystal surfaces as a function of structure imposed on the liquid by the crystals. This showed that structural constraint imposed by the crystal surfaces forced the film to be disordered at the interface because it was energetically preferred to an abrupt change in structure that would result in a large gradient energy. In this case, therefore, it might be difficult to nucleate any crystalline phase at the liquid-film region, where the glass-network molecules would be structurally constrained.

All of the explanations discussed in Sec. III for the limitations of boundary film crystallization were based on the uniform composition of liquid phase through the whole specimen. Recently, Chiang *et al.*,[24] Gu *et al.*,[25] and Brydson *et al.*,[26] independently observed the composition difference of liquid phase between two-grain and triple-junction regions. The composition difference was explained using segregation concepts of specific cations at each solid–liquid interface; these ex-

perimental results signify that the composition of film need not be identical to that of the bulk liquid located at triple junctions.

In addition to the segregation, there is also a necessity to have a viewpoint of compositional difference with respect to the microstructural difference between two-grain and triple-junction regions. The radius of the curvature of solid–liquid interface may be an important geometrical factor, which determines the chemical potential of atoms at the interface. According to the Thompson–Freundlich equation,[27] the solubility of solid particles in the liquid phase is inversely proportional to the radius of solid particles. Because the curvatures of solid particle at triple junction regions are small compared with two-grain junction that have flat boundary morphology, the solubility of solid particles in the liquid phase at triple junction regions are also higher than those at the two-grain junction as shown in Fig. 5. Concerning the concentration of solute at triple junction, Greenwood[27] and others[28,29] have demonstrated the concentration gradient profile of a solute with distance. The approximate formula derived to predict the solute concentration gradient around each particle showed that the effective influential distance of concentration to be the radius of the solute particle from the surface. Under this condition, the concentration profiles of each particle at triple-junction overlap with each other, and a higher concentration due to higher solubility is expected.

When a new phase is formed by a nucleation and growth process in a liquid, we can consider factors such as supercooling, degree of supersaturation, and viscosity. If we consider the effect of increasing supersaturation at a constant temperature, the rate of nucleation is very sensitive to the degree of supersaturation especially when the supersaturation approaches some critical value.[30] On the other hand, the viscosity of a liquid should also be considered as an important factor. The Stokes–Einstein relation,[31] which is frequently used to estimate the atom diffusivity in a viscous melt, shows that the diffusion coefficient is inversely proportional to viscosity. Thus, the nucleation rate is inversely proportional to viscosity because high viscosity reduces the jump frequency of atoms, i.e., a lower viscosity of liquid with the dissolution of certain components into liquid phases increases the nucleation rate.[32]

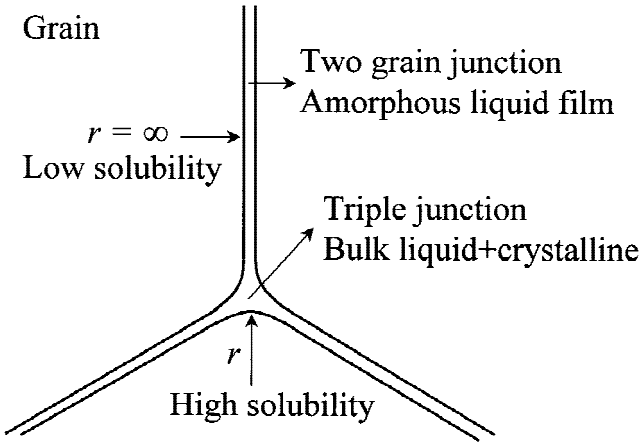

FIG. 5. Schematic representation of a triple junction with liquid films.

During the sintering process, in our system, the BaB_2O_4 phase will melt at the eutectic temperature and some of the Ti and Ba ions will be concurrently dissolved into BaB_2O_4 melts from $BaTiO_3$ grains, and then form Ba–Ti–B–O glass. In Ba–Ti–B–O glass, B and Ba components act as glass network former and modifier, respectively. Thus, the dissolving of Ba and Ti components may lead to the lowering of the viscosity of the liquid and supersaturation of glass with Ba and Ti components concurrently. Since the radius of curvature in solid–liquid interface is small at the liquid pocket, the amount of dissolved Ba and Ti components is also large compared with the liquid film. When the specimen was cooling down after sintering, the crystallization of BaB_2O_4 was thought to occur at the bulk-liquid pocket located at triple junctions, which had rather low viscosity and high supersaturation, compared with the liquid film at two-grain junction. Therefore, such a high solubility of solid particles at triple junctions into the liquid phase may accelerate the crystallization of the liquid phase during the cooling process.

IV. CONCLUSION

Two kinds of distribution characteristics of boundary phases in BaB_2O_4 added $BaTiO_3$ ceramics were observed by HRTEM: (i) triple junction filled with a mixture of liquid phase and crystallized BaB_2O_4 phase, and (ii) two-grain junction with a flat amorphous thin film. This kind of boundary phase distribution characteristic was explained with a viewpoint of compositional difference with respect to the microstructure difference between two-grain and triple-junction regions. Because the solubility of solid particles in the liquid phase are inversely proportional to the radius of solid particles, the solid particle at the triple-junction region has smaller curvature and are more soluble than the two-grain junction. Such a high solubility of a solid particle to the liquid phase concurrently leads to supersaturation of the glass phase and lowers the viscosity of the liquid, which eventually accelerates crystallization of the liquid phase during the cooling process.

ACKNOWLEDGMENT

The authors greatly appreciate the helpful advice of Prof. Yet-Ming Chiang at the Department of Materials Science and Engineering, MIT, Cambridge, MA.

REFERENCES

1. O. Saburi, J. Phys. Soc. Jpn. **14,** 1157 (1959).
2. G.H. Jonker, Mater. Res. Bull. **2,** 401 (1967).
3. J-H. Lee, S-H. Kim, and S-H. Cho, J. Am. Ceram. Soc. **78,** 2845 (1995).
4. Y. Matsuo, M. Fujimura, H. Sasaki, K. Nagase, and S. Hayakawa, Ceram. Bull. **47,** 292 (1968).
5. H.F. Cheng, J. Appl. Phys. **66,** 1382 (1989).
6. V. Ravi and T.R.N. Kutty, J. Am. Ceram. Soc. **75,** 203 (1992).
7. S-J. Park, J-H. Lee, and S-H. Cho, in *Grain Boundaries and Interfacial Phenomena in Electronic Ceramics*, edited by L.M. Levinson and S. Hirano (Ceram. Trans. **41,** The American Ceramic Society, 1994), pp. 145–51.
8. I.C. Ho, J. Am. Ceram. Soc. **77,** 829 (1994).
9. Y-W. Heo, J-H. Lee, J-J. Kim, N-K. Kim and S-H. Cho, J. Kor. Ceram. Soc. **33,** 1038 (1996).
10. H.H. Park and D.N. Yoon, Metall. Trans. A **16A,** 923 (1985).
11. P.J. Wray, Acta Metall. **24,** 125 (1976).
12. K.W. Lay, J. Am. Ceram. Soc. **51,** 373 (1968).
13. D.R. Clarke, J. Am. Ceram. Soc. **70,** 15 (1987).
14. H-J. Kleebe, M.J. Hoffmann, and M. Rühle, Zeitschrift für Metallkunde **83,** 610 (1992).
15. Y-M. Chiang, L.A. Silverman, R.H. French, and R.M. Cannon, J. Am. Ceram. Soc. **77,** 1143 (1994).
16. Phase Diagrams for Ceramists 1975 Supplement, Vol. 3, Fig. 4545, edited and published by The American Ceramic Society (1975).
17. D.R. Clarke, T.M. Shaw, A.P. Philipse, and R.G. Horn, J. Am. Ceram. Soc. **76,** 1201 (1993).
18. R. Raj, in *Tailoring of Mechanical Properties of Si_3N_4 Ceramics*, edited by M.J. Hoffmann, and G. Petzow (NATO Asi Series E, Kluwer Academic Publishers, Boston, MA, 1994), Vol. 276, pp. 201–206.
19. R. Raj, J. Am. Ceram. Soc. **64,** 245 (1981).
20. R. Raj and F.F. Lange, Acta Metall. **29,** 1993 (1981).
21. H. Kessler, H-J. Kleebe, R.M. Cannon, and W. Pompe, Acta Metall. Mater. **40,** 2233 (1992).
22. M.M. Chadwick, R.S. Jupp, and D.S. Wilkinson, J. Am. Ceram. Soc. **76,** 385 (1993).
23. H.D. Ackler, Ph.D. Thesis, Massachusetts Institute of Technology, Cambridge, MA, (1997).
24. Y-M. Chiang, L.A. Silverman, R.H. French, and R.M. Cannon, J. Am. Ceram. Soc. **77,** 1143 (1994).
25. H. Gu, X. Pan, R.M. Cannon, and M. Rühle, J. Am. Ceram. Soc. **81,** 3125 (1998).
26. R. Brydson, S-C. Chen, F.L. Riley, S.J. Milne, X. Pan, and M. Rühle, J. Am. Ceram. Soc. **81,** 369 (1998).
27. G.W. Greenwood, Acta Metall. **4,** 243 (1956).
28. J.M. Lifshitz and V.V. Slyozov, J. Phys. Chem. Solids **19,** 35 (1961).
29. A.J. Ardell, Acta Metall. **20,** 61, (1972).
30. J.W. Christian, *The Theory of Transformations in Metals and Alloys*, 2nd ed. (Pergamon Press, Oxford, United Kingdom, 1981), p. 431.
31. Y-M. Chiang, D.P. Birnie, III, and W.D. Kingery, *Physical Ceramics*, (Wiley & Sons, New York, 1997), p. 434.
32. D.R. Uhlmann and N.J. Kreidl, *Glass Forming Systems*, Glass Science and Technology Vol. 1 (Academic Press, New York, 1983), p. 8.